Identification of Variant Molecules of *Bacillus thermoproteolyticus* Ferredoxin: Crystal Structure Reveals Bound Coenzyme A and an Unexpected [3Fe−4S] Cluster Associated with a Canonical [4Fe−4S] Ligand Motif[†,‡]

Tadayoshi Shirakawa,[§] Yasuhiro Takahashi,[§] Kei Wada,[§] Junko Hirota,[||] Toshifumi Takao,[||] Daijiro Ohmori,[⊥] and Keiichi Fukuyama*[,§]

Department of Biology, Graduate School of Science, Osaka University, 1-1 Machikaneyama, Toyonaka, Osaka 560-0043, Japan, Institute for Protein Research, Osaka University, 2-2 Yamadaoka, Suita, Osaka 565-0871, Japan, and Department of Chemistry, Juntendo University, Inba, Chiba 270-1695, Japan

Received May 6, 2005; Revised Manuscript Received July 28, 2005

ABSTRACT: During the purification of recombinant *Bacillus thermoproteolyticus* ferredoxin (BtFd) from *Escherichia coli*, we have noted that some Fe−S proteins were produced in relatively small amounts compared to the originally identified BtFd carrying a [4Fe−4S] cluster. These variants could be purified into three Fe−S protein components (designated as V-I, V-II, and V-III) by standard chromatography procedures. UV−vis and EPR spectroscopic analyses indicated that each of these variants accommodates a [3Fe−4S] cluster. From mass spectrometric and protein sequence analyses together with native and SDS gel electrophoresis, we established that V-I and V-II contain the polypeptide of BtFd associated with acyl carrier protein (ACP) and with coenzyme A (CoA), respectively, and that V-III is a BtFd dimer linked by a disulfide bond. The crystal structure of the BtFd−CoA complex (V-II) determined at 1.6 Å resolution revealed that each of the four complexes in the crystallographic asymmetric unit possesses a [3Fe−4S] cluster that is coordinated by Cys^{11}, Cys^{17}, and Cys^{61}. The polypeptide chain of each complex is superimposable onto that of the original [4Fe−4S] BtFd except for the segment containing Cys^{14}, the fourth ligand to the [4Fe−4S] cluster of BtFd. In the variant molecules, the side chain of Cys^{14} is rotated away to the molecular surface, forming a disulfide bond with the terminal sulfhydryl group of CoA. This covalent modification may have occurred *in vivo*, thereby preventing the assembly of the [4Fe−4S] cluster as observed previously for *Desulfovibrio gigas* ferredoxin. Possibilities concerning how the variant molecules are formed in the cell are discussed.

Ferredoxins (Fds)[1] are small, generally acidic, electron-transfer proteins that function in diverse biological redox systems (*1*−*5*). They contain iron−sulfur (Fe−S) clusters in [2Fe−2S], [3Fe−4S], and [4Fe−4S] forms that are ligated to the polypeptide primarily via cysteine residues. Among them, Fds containing one or two [4Fe−4S] (or [3Fe−4S]) clusters are evolutionally related and categorized as bacteria-type Fds, distinct from the [4Fe−4S] HiPIPs or [2Fe−2S] Fds (*6*−*8*). The cluster most common in bacteria-type Fds is the cubane [4Fe−4S] form, with three of the four cysteine ligands of the [4Fe−4S] cluster provided by a canonical Fe−S-binding motif Cys-X-X-Cys-X-X-Cys. The [4Fe−4S] cluster is located near the edge of the Fd molecule, where the cluster is shielded from the solvent by the main-chain atoms of the binding motif. Furthermore, the main-chain NH groups of the consensus sequence are directed toward the [4Fe−4S] cluster and participate in NH···S hydrogen bonds.

The other type of Fe−S cluster observed in bacterial Fds is the [3Fe−4S] type, which differs only in the absence of a single Fe atom at one corner of the cube. Interconversion between 3Fe and 4Fe clusters is well-known to occur in a certain class of Fe−S proteins. This is best illustrated by aconitase, in which the [3Fe−4S] cluster is inactive and its conversion to [4Fe−4S] represents a self-activation of the enzyme (*9*, *10*). Fe−S proteins that undergo facile cluster conversion have, in general, three cysteine and one noncysteine ligand to the [4Fe−4S] cluster. The noncysteine ligand of aconitase is water or OH^-. Similarly, a subgroup of bacteria-type Fds, which also easily interconvert, has a Cys-X-X-Asp-X-X-Cys motif in which aspartate serves as the fourth ligand (*11*−*14*). In contrast, most [4Fe−4S] clusters have four cysteine ligands and do not undergo cluster interconversion; the cluster can be converted to the [3Fe−4S] state only during destructive reactions leading to the

[†] This work was supported in part by a grant of the National Project on Protein Structural and Functional Analyses to K.F. and by a Grant-in-Aid for Scientific Research to Y.T. (number 15510174) from the Ministry of Education, Culture, Sports, Science, and Technology of Japan.

[‡] Coordinates and structure factors have been deposited in the Protein Data Bank, accession code 1WTF.

* To whom correspondence should be addressed. Telephone: +81-6-6850-5422. Fax: +81-6-6850-5425. E-mail: fukuyama@bio.sci.osaka-u.ac.jp.

[§] Graduate School of Science, Osaka University.

[||] Institute for Protein Research, Osaka University.

[⊥] Juntendo University.

[1] Abbreviations: ACP, acyl carrier protein; BtFd, ferredoxin from *Bacillus thermoproteolyticus*; CoA, coenzyme A; DgFd, ferredoxin from *Desulfovibrio gigas*; EPR, electron paramagnetic resonance; Fd, ferredoxin; Fe−S, iron−sulfur.

10.1021/bi0508441 CCC: $30.25
Published on Web 08/26/2005

apoprotein (*12*, *15*−*17*). The only exception to this rule is *Desulfovibrio gigas* Fd (DgFd), which possesses the canonical Cys-X-X-Cys-X-X-Cys motif but can still undergo interconversion of its Fe−S cluster (*18*−*21*).

It is generally thought that the spatial arrangement of the liganding amino acids and neighboring residues determine the Fe−S cluster type, although the assembly of Fe−S clusters and their insertion into apo-Fe−S proteins are complex processes that are not yet fully understood. Recent genetic and biochemical studies have revealed three distinct systems that are involved in Fe−S cluster biosynthesis, termed NIF, ISC, and SUF (for recent reviews, *22*−*24*). The three systems show mechanistic similarity in their requirement for a cysteine desulfurase (sulfur donor) as well as scaffold proteins to form transient Fe−S clusters. More recently, *in vivo* experiments have demonstrated interchangeability among the three systems, suggesting that they all are responsible for maturation of a wide variety of Fe−S proteins without strict specificity for apoprotein targets or Fe−S cluster types (*25*−*27*). Little is known, however, about the delivery of Fe−S clusters to their target apo-Fe−S proteins or the role of the Cys-X-X-Cys-X-X-Cys motif in this process. Although direct cluster transfer between scaffold proteins and apo-Fds has been demonstrated in simplified *in vitro* experiments, this process apparently requires additional components for successful completion *in vivo*.

For several years, we have used a ferredoxin from *Bacillus thermoproteolyticus* (BtFd) as a model of monocluster Fds to address several basic questions regarding the biosynthesis of Fe−S proteins as well as their structure−function relationships. BtFd is a simple and highly stable Fe−S protein that contains a single [4Fe−4S] cluster and only four cysteine residues (three cysteine residues in the canonical Cys^{11}-X-X-Cys^{14}-X-X-Cys^{17} motif and a remote Cys^{61} residue), which all participate in cluster coordination. Expression of the BtFd gene in *Escherichia coli* results in high levels of holo-BtFd synthesis, particularly when coexpressed with the *isc* gene cluster (*iscSUA-hscBA-fdx*), which boosts Fe−S cluster assembly (*28*, *29*). Previously, we purified recombinant BtFd and determined its crystal structure at atomic (0.92 Å) resolution (*30*). In the course of these studies, we have repeatedly observed contaminating reddish brown proteins that are not seen in the absence of the BtFd expression plasmid. Here, we report the identification of these reddish brown proteins, which we have separated into three fractions by multiple purification steps. From our analysis, we have identified the three proteins as variant molecules of BtFd carrying the [3Fe−4S] cluster instead of the [4Fe−4S] type. Furthermore, two of the fractions represent Fd variants that are associated with either acyl carrier protein (ACP) or coenzyme A (CoA). These are the first examples of such variants to be discovered. Additionally, the crystal structure of the BtFd−CoA complex clearly shows that the central cysteine residue in the Cys-X-X-Cys-X-X-Cys motif is covalently modified by a terminal sulfhydryl group of CoA.

EXPERIMENTAL PROCEDURES

Expression and Purification of BtFd Variant Molecules. The BtFd gene was constructed from synthetic oligonucleotides based on the published amino acid sequence and the optimal codon usage of *E. coli* (K. Saeki, unpublished). The BtFd gene was cloned into the plasmid pET-21a(+) and coexpressed with the *isc* operon in *E. coli* strain C41(DE3) to produce holo-BtFd in high yield (*28*, *29*). The bacteria were cultivated in 4 L of Terrific broth containing 100 μg/mL ampicillin, 5 μg/mL tetracycline, and 0.1 mg/mL ferric ammonium citrate. Expression was induced with 0.5 mM IPTG, and the cells were further grown for 20 h at 28 °C. The cells were pelleted and then suspended in a solution containing 50 mM Tris-HCl at pH 7.8, 0.1% Triton X-100, and 0.1 mg/mL lysozyme. After incubation at 30 °C for 30 min, the cells were disrupted by sonication. The suspension was centrifuged at 12000*g* for 1 h at 4 °C; the supernatant was loaded onto a DEAE-cellulose column; and the bound acidic proteins were eluted with 50 mM Tris-HCl at pH 7.8 containing 700 mM NaCl. The colored fractions thus obtained were subjected to ammonium sulfate fractionation at 60% saturation. After centrifugation, the supernatant fraction was applied onto a Butyl-Toyopearl 650-M column (TOSOH) and eluted with a linear gradient of ammonium sulfate (55−25%) in 50 mM Tris-HCl at pH 7.8. In this hydrophobic chromatography, a reddish brown fraction was separated from a grayish brown fraction, with the latter containing the original [4Fe−4S] BtFd. The reddish brown fraction was dialyzed against a solution containing 50 mM Tris-HCl at pH 7.8 and 0.1 M NaCl, applied to an anion-exchange column (DEAE-Toyopearl 650-M, TOSOH), and eluted with a linear gradient of NaCl (100−400 mM). The reddish brown proteins, separated into two fractions, were further purified by gel-filtration (Sephacryl S-200) and anion-exchange (Mono Q HR 5/5) chromatography using an ÄKTA explorer 10S (Amersham Biosciences). The purification scheme is diagrammed in Figure 1.

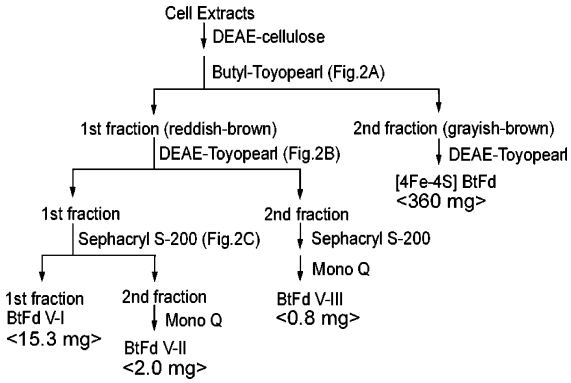

FIGURE 1: Purification scheme for [4Fe−4S] BtFd and the three variant molecules. Typical purification yields from *E. coli* cells (approximately 120 g) are indicated in square brackets.

Analytical Methods. Concentrations of the BtFd molecular variants were determined by the method of Bradford (*31*) using purified [4Fe−4S] BtFd as a standard. SDS−PAGE (15% gel) and native−PAGE (22.5% gel) were carried out according to the methods of Laemmli (*32*) and Davis (*33*), respectively. The N-terminal amino acid sequence of the 17-kDa protein constituent of BtFd V-I was determined using a G1000A protein sequencer (Hewlett Packard). UV−vis absorption spectra were recorded with a UV-3101 PC UV−vis scanning spectrophotometer (Shimadzu). The dynamic light-scattering characteristics of protein solutions were analyzed using a DynaPro-99 molecular-sizing detector (Protein Solutions). Electron paramagnetic resonance (EPR) spectra were obtained on a JES-FE3XG spectrometer (JEOL)

equipped with an RMS model CT-470-ESR cryostat system and a Scientific Instruments model 9650 temperature controller. Recording conditions were as follows: microwave power, 0.05 mW; modulation amplitude, 0.63 mT; and temperature, 8.5 K. Mass spectra of proteins were obtained by electrospray ionization mass spectrometry using a hybrid quadruple orthogonal acceleration tandem mass spectrometer (Micromass). Samples were infused at a flow rate of 10−20 nL/min, with concentrations ranging from 50 fmol/μL to 1 pmol/μL. Spectra were acquired and processed with MaxEnt3 (Micromass).

Crystallization and Intensity Data Collection of BtFd V-II. Crystallization of BtFd V-II was conducted by the hanging drop vapor diffusion method using ammonium sulfate as the precipitant. Crystals were produced upon mixing ~10 mg/mL V-II solution in 50 mM Tris-HCl at pH 7.8, 100 mM NaCl, and 4% acetonitrile with reservoir solution (3.2 M ammonium sulfate and 0.1 M Tris-HCl at pH 8.0) in a 1:1 ratio with subsequent equilibration at 4 °C. Rod-shaped crystals appeared after a couple of days and were transferred to a cryoprotectant solution (3.6 M ammonium sulfate in 0.1 M Tris-HCl at pH 8.0) and flash-cooled in a nitrogen gas stream at 100 K. Two sets of X-ray diffraction data for V-II were collected at SPring-8 using synchrotron radiation at beamline BL41XU with a MAR CCD detector. Data were collected at $\lambda = 1.50$ Å for phasing by the single wavelength anomalous scattering of iron atoms present in the Fe−S protein and at $\lambda = 1.00$ Å for structural refinement at high resolution. All data were processed using the software package HKL 2000 (*34*). The BtFd V-II crystals belonged to the space group $P2_1$, with the unit-cell constants $a = 52.4$ Å, $b = 63.4$ Å, $c = 56.9$ Å, and $\beta = 95.1°$ at 100 K.

Structure Determination and Refinement of BtFd V-II. The molecular replacement method was applied using the BtFd structure (PDB entry 1IQZ), from which the Fe−S cluster and solvent molecules were excluded, as a search model for MOLREP (*35*). From this procedure, three of four crystallographically independent molecules in an asymmetric unit were located. The atomic coordinates of the three molecules were used to calculate the phase angles, which were combined with the Bijvoet differences collected at $\lambda = 1.50$ Å. The resultant difference map revealed four three-iron clusters. Three of the four clusters were at the expected sites in the molecules determined by the molecular replacement, establishing the iron sites. The phase angles were derived on the basis of the four three-iron clusters by the single anomalous scattering method to produce the map from which the polypeptide chain of the fourth molecule was traced. The structure was refined using the data collected at $\lambda = 1.00$ Å with CNS (*36*), and the model was revised manually with O (*37*). The model was then improved by alternating rounds of refinement and model-building until the R_{free} value was reduced to 25%. At this stage, ordered water molecules were added to the BtFd structure. Then, the $F_o - F_c$ map was scrutinized to determine the location of CoA; one of the four CoA moieties was entirely visible, whereas the other three were only partially so. The [3Fe−4S] cluster geometry was not restrained in the refinement. The structure of BtFd V-II was refined to a final crystallographic *R* factor of 0.18 and R_{free} of 0.21 for the data to 1.6 Å resolution. The quality of the model was analyzed with PROCHECK (*38*). Data collection and refinement statistics are shown in Table 1.

Table 1: Data Collection and Refinement Statistics for the BtFd−CoA

Data Collection Statistics[a]		
wavelength (Å)	1.500	1.000
resolution limit (Å)	50.0−2.4 (2.47−2.4)	33.9−1.6 (1.68−1.6)
completeness (%)	95.9 (90.2)	98.5 (98.5)
number of unique reflections	28 206	49 210
redundancy	3.0 (2.1)	3.5 (2.6)
mean I/σ	12.8 (7.8)	7.5 (6.1)
R_{sym} (%)[b]	7.9 (10.9)	6.2 (10.7)
Refinement and Model Statistics		
resolution range for refinement (Å)		31.8−1.6
number of monomers per asymmetric unit		4
number of unique reflections (excluding the test set)		48 081 (43 237)
crystallographic *R* factor[c] (R_{free})		0.178 (0.211)
number of molecules		
CoA		1
SO_4^{2-}		3
water		779
rms deviations from ideal values		
bond length (Å)		0.020
bond angles (deg)		2.0
average *B* factor (Å^2)		17.3

[a] Number in parentheses corresponds to the highest-resolution shell. [b] $R_{sym} = (\sum_{hkl}\sum_i|I_i(hkl) - \langle I(hkl)\rangle|)/\sum_{hkl}\sum_i I_i(hkl)$. [c] R factor$=\sum_{hkl}||F_o(hkl)| - |F_c(hkl)||/\sum_{hkl}|F_o(hkl)|$.

RESULTS AND DISCUSSION

Purification of BtFd Variant Molecules. While purifying the recombinant BtFd from *E. coli*, we repeatedly observed proteins significantly different in color from [4Fe−4S] BtFd. Upon fractionation, the first fraction eluting from the hydrophobic butyl column appeared reddish brown, followed by a fraction displaying normal grayish brown color indicative of native [4Fe−4S] BtFd (Figure 2A). To determine whether the reddish brown color arose from an unusual form of BtFd or from a contaminating protein, this protein fraction was purified to homogeneity. As diagrammed in Figure 1, the reddish brown proteins were ultimately separated into three fractions by successive chromatography on anion-exchange and gel-filtration columns (parts B and C of Figure 2). Because all three fractions contained the BtFd polypeptide as described below, we designated them as BtFd V-I, V-II, and V-III (variant molecules of BtFd). A typical purification yielded 15.3 mg of V-I, 2.0 mg of V-II, and 0.8 mg of V-III from 4 L of culture (about 120 g of cell paste), very small amounts compared with typical yields of [4Fe−4S] BtFd (360 mg) from the same size preparation. It should be noted that BtFd V-II eluted from the size-exclusion column virtually at the same elution volume as [4Fe−4S] BtFd, whereas the V-I and V-III fractions eluted earlier, indicating that they possessed greater molecular mass (Figure 2C and not shown). However, precise determination of these molecular masses was complicated by the fact that [4Fe−4S] BtFd (9117 Da) behaves abnormally on a gel-filtration column, eluting as if its molecular weight were 21 000. The molecular masses estimated by dynamic light scattering were 9.7 kDa for [4Fe−4S] BtFd, 19.2 kDa for BtFd V-I, 8.2 kDa for V-II, and 16.4 kDa for V-III.

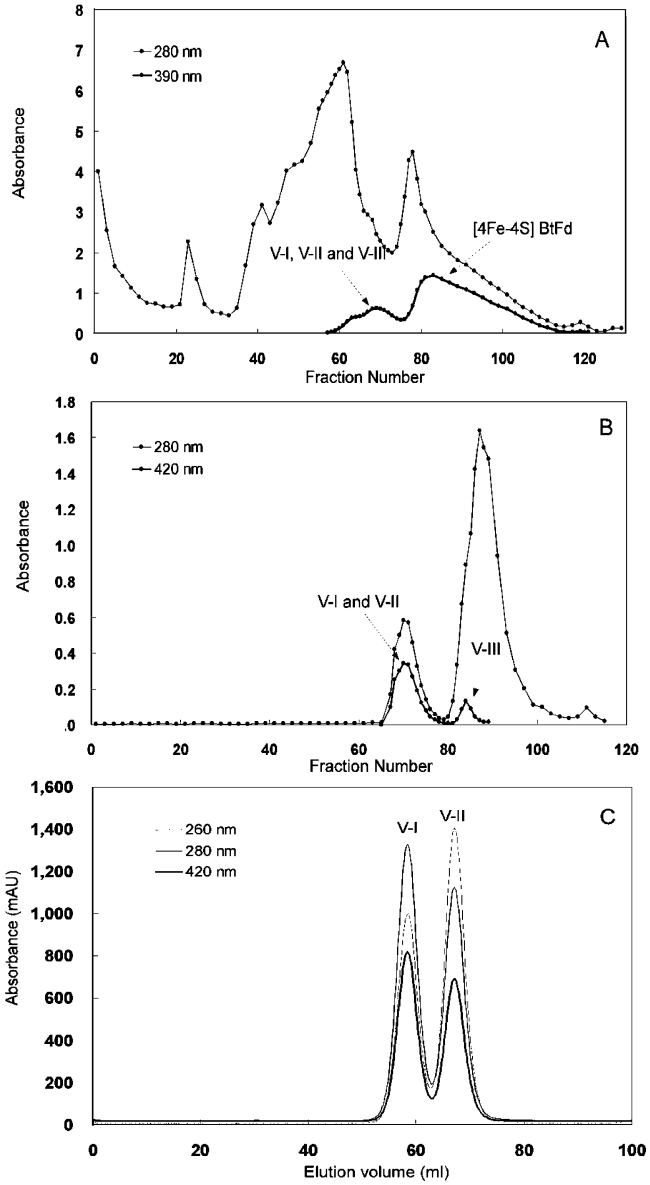

FIGURE 2: Separation and purification of the variant molecules of BtFd. (A) Hydrophobic chromatography on a Butyl-Toyopearl 650-M column. (B) Anion-exchange chromatography on a DEAE-Toyopearl 650-M column. (C) Gel-filtration chromatography on a Sephacryl S-200 column. For details, see the Experimental Procedures. Elution of proteins, Fe−S proteins, and nucleotides were monitored by absorbance at 280, 390 (or 420), and 260 nm, respectively.

Constituents in BtFd Variant Molecules. The purified variant molecules of BtFd migrated on a nondenaturing native gel as single bands, but their mobility was different from each other and also from the original [4Fe−4S] BtFd (Figure 3A). BtFd V-II ran on the gel slightly slower than [4Fe−4S] BtFd, while the larger molecules, V-I and V-III, displayed significantly slower migration. From SDS gel electrophoresis (Figure 3C), however, BtFd V-II and V-III migrated as single bands identical to that of [4Fe−4S] BtFd. BtFd V-I displayed two bands by SDS−PAGE, one corresponding to BtFd and the other to a 17-kDa polypeptide. To identify this 17-kDa protein, we electrotransferred it onto a PVDF membrane following separation by SDS−PAGE and sequenced its amino terminus. The resulting sequence was determined to be STIEERVKKIIGEQLGVKQE, which is identical to the N-terminal sequence of *E. coli* ACP. ACP is composed of 77 residues and is modified by covalent attachment of a 4′-phosphopantetheine prosthetic group to the hydroxyl group of residue Ser[36] by phosphodiester linkage. Although the low molecular mass of ACP (8847 Da including the 4′-phosphopantetheine moiety) is inconsistent with that observed by SDS−PAGE (17 kDa), such anomalous behavior has previously been reported (*39*, *40*).

For further identification of the BtFd variants, we determined their molecular masses by electrospray ionization mass spectrometry. The deconvolution of the mass spectrum of BtFd V-I revealed three molecular masses, 8768, 8849, and 17 617 Da, which can be attributed to the BtFd polypeptide (8769 Da), holo-ACP (8847 Da), and the sum of the two proteins (17 616 Da), respectively. Thus, BtFd V-I is composed of two proteins, BtFd and holo-ACP, carrying the 4′-phosphopantetheine moiety. The molecular masses also suggest that these proteins form a covalently bound complex in an equimolar ratio. BtFd V-II displayed molecular masses of 8768 and 9536 Da, corresponding to the BtFd polypeptide and to a complex of the BtFd polypeptide and CoA (738 Da), respectively. The identification of the BtFd−CoA complex is consistent with the absorption spectrum of BtFd V-II and was further confirmed by the crystal structure (see below). For BtFd V-III, no molecules other than BtFd were detected. The larger molecular masses observed in the gel-filtration and dynamic light-scattering experiments suggest that the BtFd V-III molecule is most likely a homodimer of BtFd.

All three of the BtFd variants were separated into their respective molecular constituents in the presence of a reducing reagent. As shown in Figure 3B, DTT treatment resulted in dissociation of the BtFd−ACP complex (BtFd V-I) into ACP and BtFd polypeptides, the latter of which migrated on a nondenaturing gel at the same position as [4Fe−4S] BtFd. Likewise, the mobility shift was observed for BtFd V-II and V-III after DTT treatment. In a parallel experiment using analytical Mono Q chromatography, the individual components of BtFd V-II, CoA and BtFd, were both detectable following DTT treatment of this variant (not shown). These results clearly indicate that the BtFd polypeptides of the V-I and V-II molecules are covalently bound via disulfide linkage to ACP and CoA, respectively. Disulfide bonding may also be involved in the dimerization of BtFd in V-III. Intriguingly, BtFd contains only 4 cysteine residues per molecule, all of which are involved in the coordination of the Fe−S cluster in the original [4Fe−4S] BtFd.

Each BtFd Variant Molecule Contains a [3Fe−4S] Cluster. The variant molecules of BtFd show UV−vis absorption spectra that are distinct from those obtained for [4Fe−4S] BtFd (Figure 4). However, the spectra of the three variant molecules are almost indistinguishable from each other and are indeed identical in the visible region above 350 nm, with a broad maximum at 415 nm and a shoulder at around 455 nm. Similar spectral features have been reported previously for [3Fe−4S] proteins, such as DgFd (*41*). The peak at 260 nm observed for BtFd V-II is consistent with the presence of a nucleotide moiety (CoA) as described above. Upon reduction with dithionite, the absorbances in the visible region were greatly reduced, and the spectra of the oxidized forms were recovered when the reduced molecules were exposed to air (not shown). This suggests

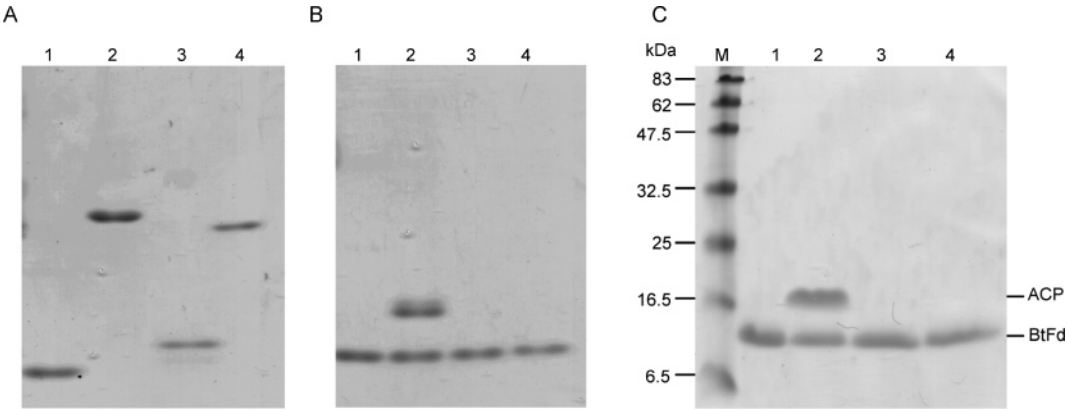

FIGURE 3: Electrophoretic analysis of the variant molecules of BtFd. Electrophoresis was carried out under nondenaturing and nonreducing conditions (A), nondenaturing conditions with 5 mM DTT (B), and denaturing conditions in the presence of 2% SDS and 2% β-mercaptoethanol (C). The gels were stained with Coomassie Blue. Lane 1, original [4Fe−4S] BtFd; lane 2, BtFd V-I; lane 3, V-II; and lane 4, V-III. Lane M indicates size-marker proteins.

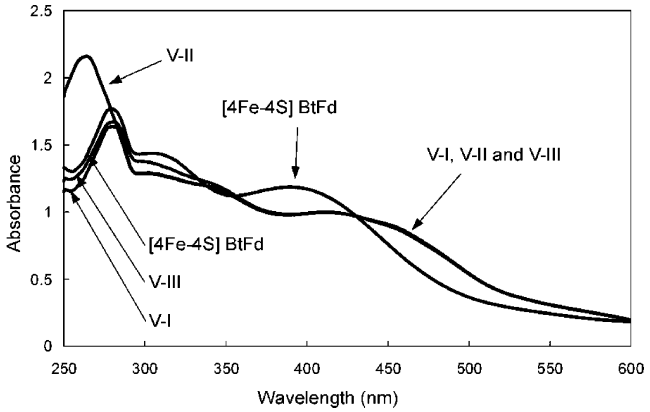

FIGURE 4: UV−vis absorption spectra of the BtFd variant molecules and [4Fe−4S] BtFd. Samples were dissolved in 50 mM Tris-HCl buffer at pH 7.8 containing 0.1 M NaCl. The spectra were recorded at room temperature and normalized at 410 nm to facilitate a comparison.

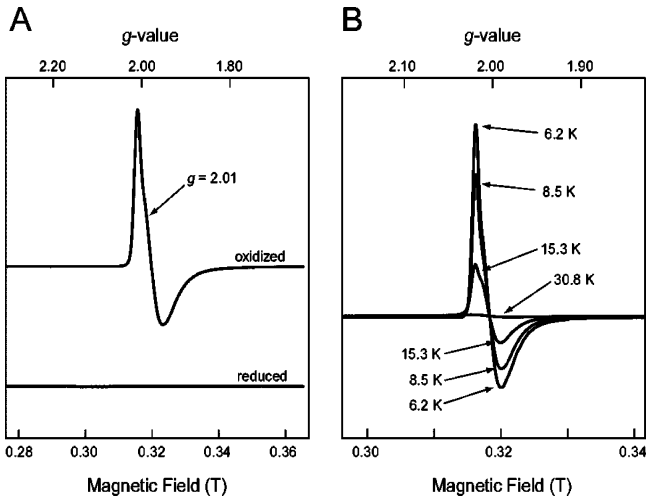

FIGURE 5: EPR spectra of BtFd variant molecule V-I. (A) Comparison between oxidized (as isolated) and dithionite-reduced BtFd V-I measured at 8.5 K. (B) Temperature-dependent signal intensity of the oxidized BtFd V-I. Both spectra were measured under the following conditions: microwave power, 0.05 mW; modulation width, 0.63 mT.

that the Fe−S clusters are redox-active and also stable in the presence of dithionite or O_2.

EPR analysis of the oxidized form of the [4Fe−4S] BtFd yielded no signal. Upon reduction by dithionite, the spectrum exhibited signals with apparent *g* values of 2.06, 1.93, and 1.89 (data not shown), which are characteristic of the reduced [4Fe−4S] cluster and identical to the values reported previously for this class of Fds (*42*). In marked contrast to the [4Fe−4S] BtFd, the BtFd variants (V-I as a representative) were EPR-silent following reduction with dithionite (Figure 5A). Instead, BtFd V-I exhibited an EPR signal centered at $g = 2.01$ in the oxidized form, which is typical of [3Fe−4S] clusters and has been demonstrated for a number of [3Fe−4S] proteins (*43*). The EPR signal from oxidized BtFd V-I showed an optimum as low as 6 K with marked broadening at 15 K, finally disappearing at 30 K (Figure 5B). The temperature dependence of the EPR signal provides further support that BtFd V-I contains a [3Fe−4S] cluster.

Crystal Structure of BtFd V-II (BtFd−CoA Complex). X-ray crystallographic analysis of BtFd V-II unambiguously revealed the structure of its Fe−S cluster, the residue to which CoA is bonded, and the conformational change of the polypeptide chain upon CoA binding. Although crystals were obtained for the BtFd V-I and V-II molecules, diffraction of V-I crystals was limited to low resolution. In contrast, BtFd V-II crystals diffracted to better than 1.6 Å resolution, making all BtFd polypeptide residues, the [3Fe−4S] cluster, and the CoA moiety clearly visible in the electron-density map. The ϕ and ψ angles for all nonglycine residues fall in the allowed regions of a Ramachandran plot, with 89.3% occurring within the most favored regions. The three large peaks in the map were easily attributed to iron atoms (Figure 6A). The [3Fe−4S] cluster is coordinated by Fe−Sγ bonds to three cysteines, residues 11, 17, and 61. The distances between the Fe and S atoms are in the range of 2.17−2.32 Å, and the average S−Fe−S and Fe−S−Fe angles are about 103° and 73°, respectively. Thus, BtFd V-II does contain a conventional [3Fe−4S] cluster (*14*, *20*). One CoA moiety in the asymmetric unit was clearly identified in the $F_o - F_c$ map (Figure 6C), whereas the remaining three CoA moieties were only partially visible. The structures of the BtFd polypeptides and [3Fe−4S] clusters within the asymmetric unit are identical to one another, with the CoA moiety covalently linked to BtFd via a disulfide bond between the terminal SH group of CoA and Cys^{14} of BtFd (Figure 7A). The identification of

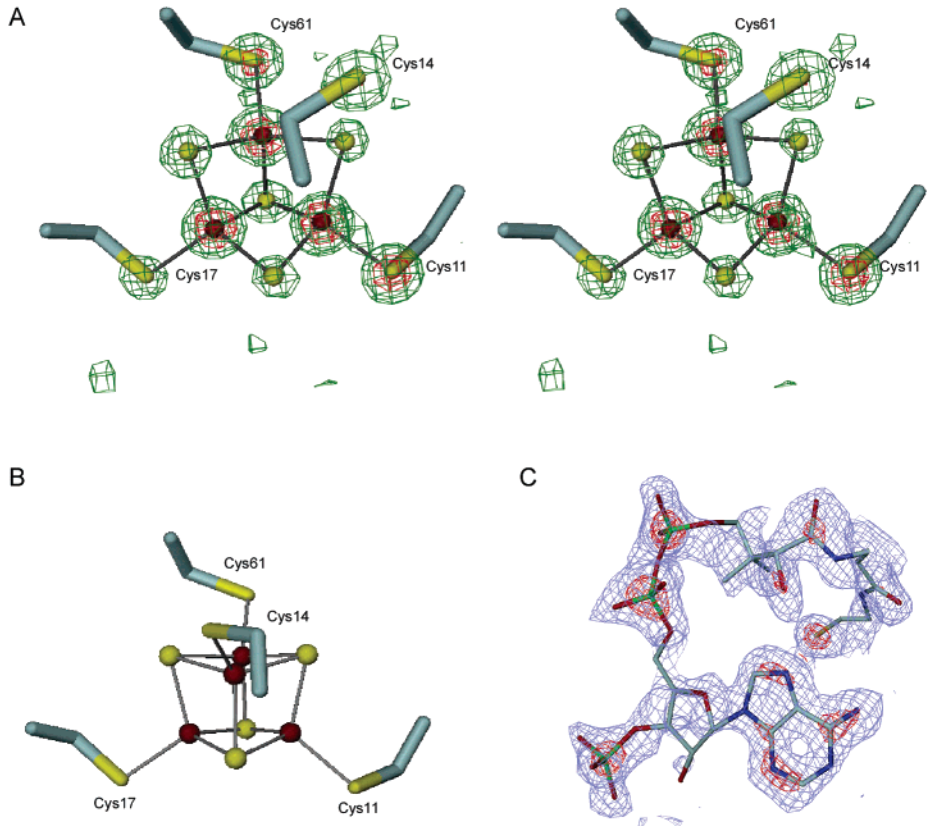

FIGURE 6: Portion of the crystal structure of BtFd V-II highlighting the [3Fe−4S] cluster and a CoA molecule. (A) Stereoview of the electron-density map around the [3Fe−4S] cluster. Red and green indicate the $2F_o - F_c$ map with contour levels of 10σ and 5σ, respectively. Fe atoms are shown in brown, and sulfur atoms are shown in yellow. The [3Fe−4S] cluster is ligated by cysteines 11, 17, and 61 in the BtFd polypeptide. (B) [4Fe−4S] cluster and the coordinating four cysteines in the original [4Fe−4S] BtFd (PDB entry 1IQZ) viewed from a similar angle as in A. (C) $2F_o - F_c$ map for the CoA moiety. The CoA moiety is superimposed on the map with red (5.0σ) and purple (1.0σ) contours. These figures were produced using DINO (http://www.dino3d.org).

the disulfide bond is consistent with the biochemical experiments described above. The CoA moiety is localized to the molecular surface, and no significant interactions are observed between the two moieties other than the disulfide linkage.

The geometry of the [3Fe−4S] cluster is virtually indistinguishable from that of the [4Fe−4S] cluster, with the exception that one Fe atom is absent at a corner of the cubic cluster (parts A and B of Figure 6). Sulfur atoms in the [3Fe−4S] cluster and Sγ atoms in the coordinating cysteine residues participate in a NH···S hydrogen-bonding network that stabilizes the cluster (*30*). Hence, the overall structure of BtFd V-II is almost identical to that of the original [4Fe−4S] BtFd, with the main-chain atoms of the two molecules superimposed with an rms deviation of 0.43 Å (Figure 7B). A conformational difference is observed only in the loop region containing the residues Cys^{14}−Ala^{16}. In the [4Fe−4S] BtFd, the distance between the Cα atoms of Cys^{14} and Cys^{61} is 8.7 Å, whereas the corresponding distance is 7.2 Å in BtFd V-II. Thus, in BtFd V-II, the loop region containing Cys^{14} moves 1.5 Å toward the Fe−S cluster to approach the empty site where the fourth iron normally resides. It should be noted that Cys^{14} is a ligand residue in [4Fe−4S] BtFd. In BtFd V-II, however, the side chain of Cys^{14} is rotated away from the [3Fe−4S] cluster and forms a disulfide bond with the terminal sulfhydryl group of CoA on the surface of the molecule (Figure 7A). The conformation of the peptide segment around the [3Fe−4S] cluster in BtFd−CoA is similar to that observed for other [3Fe−4S] Fds (Figure 7C).

Comparison with Related Ferredoxins. Some Fe−S proteins are known to bind clusters of either the [3Fe−4S] or [4Fe−4S] type, and interconversion between these types of clusters has extensively been studied for several Fds, such as *Pyrococcus furiosus* Fd, Fd III from *Desulfovibrio africanus*, and DgFd (*11*−*13*, *18*, *19*). For example, *P. furiosus* Fd and *D. africanus* Fd III possess Cys-X-X-Asp-X-X-Cys motifs, rather than the canonical [4Fe−4S]-binding motif, Cys-X-X-Cys-X-X-Cys (Figure 8). When these molecules, isolated in the [3Fe−4S] form, are subjected to reduction and addition of Fe^{2+}, the result is [4Fe−4S] cluster formation using the aspartate residue as the fourth ligand. Conversion of [4Fe−4S] to [3Fe−4S] clusters occurs during protein isolation or upon exposure to oxygen. Replacement of this aspartate with cysteine by site-directed mutagenesis results in a stable [4Fe−4S] cluster that can no longer be easily converted to [3Fe−4S] (*12*). DgFd is more closely related to BtFd, because for this molecule cluster conversion occurs despite the presence of the canonical Cys-X-X-Cys-X-X-Cys motif (Figure 8). The [3Fe−4S] cluster of DgFd can be converted to [4Fe−4S] *in vitro* by the addition of Fe^{2+} in the presence of a reducing agent (DTT), with a concomitant alteration in the oligomeric state from tetramer to dimer (*18*). Understanding the mechanism for this change in subunit composition is complicated by the fact that the [3Fe−4S] DgFd was crystallized as a monomer, although it was originally isolated as a tetramer (*20*). The crystal structure of DgFd shows that the [3Fe−4S] cluster is ligated by cysteine residues 8, 14, and 50, while a free cysteine is

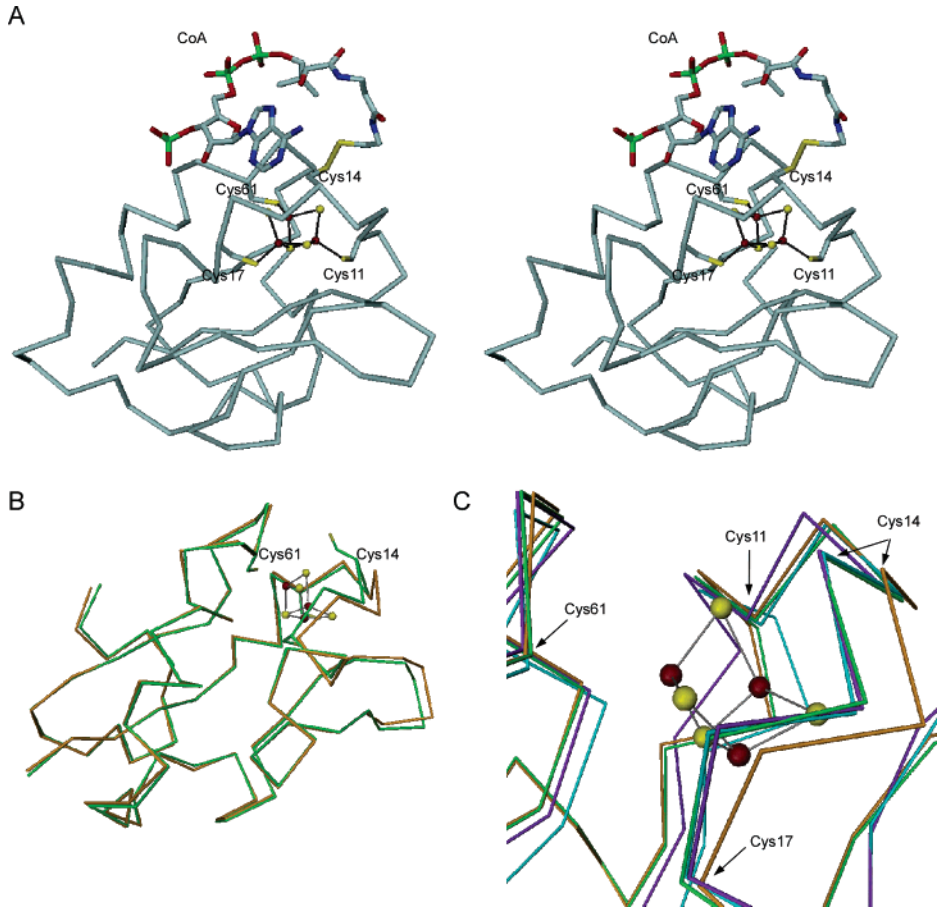

FIGURE 7: (A) Stereoview of the [3Fe−4S] BtFd−CoA complex. Four cysteine side chains and a CoA moiety are shown as stick models, in which oxygen, nitrogen, phosphorus, and sulfur atoms are shown by red, blue, green, and yellow, respectively. Iron and sulfur atoms in the Fe−S cluster are depicted as brown and yellow balls, respectively. (B) Superposition of the Cα traces of the BtFd−CoA complex (green) and the original [4Fe−4S] BtFd (orange). The [3Fe−4S] cluster of the BtFd−CoA complex is indicated in the CPK (Corey Pauling Kultin) mode. The CoA molecule in the BtFd−CoA complex and the [4Fe−4S] cluster of the original BtFd are omitted for simplicity. (C) Superposition of the Cα traces of the [3Fe−4S] Fds with [4Fe−4S] BtFd near the Fe−S cluster-binding sites. For clarity, only the cluster and the residue numbers of the BtFd−CoA complex are shown. The same colors as in B are used for BtFd−CoA, [4Fe−4S] BtFd, and [3Fe−4S] cluster. *D. gigas* Fd (PDB entry 1FXD) and *P. furiosus* Fd (PDB entry 1SIZ) are colored in purple and blue, respectively. These figures were produced with DINO. The superposition views were produced using LSQKAB (*52*).

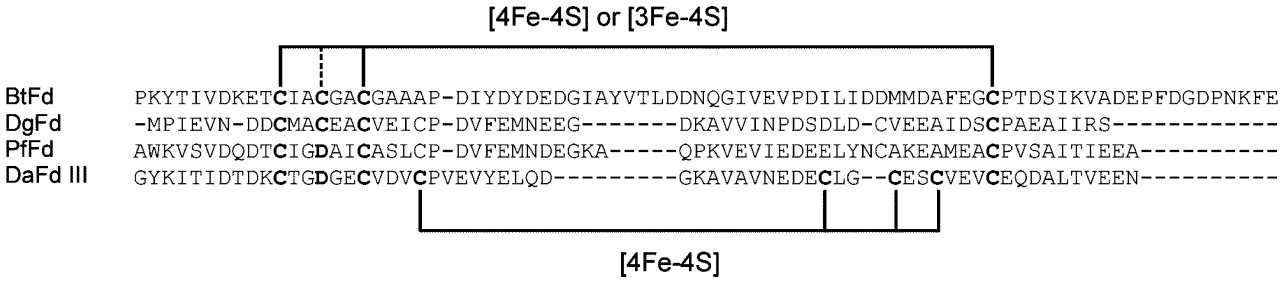

FIGURE 8: Comparison of the amino acid sequences of Fds from *B. thermoproteolyticus*, *D. gigas*, *P. furiosus*, and Fd III from *D. africanus*. These Fds may bind either [3Fe−4S] or [4Fe−4S] clusters. *D. africanus* Fd III accommodates two Fe−S clusters; one is a stable [4Fe−4S] cluster and the other undergoes cluster conversion.

present at position 11 (corresponding to Cys^{14} in BtFd). As is the case for BtFd V-II, the side chain of Cys^{11} in DgFd is rotated away from the cluster and appears to be covalently modified by a nonproteinous molecule at the surface of the protein, thus preventing it from serving as a ligand. No chemical experiments were attempted to identify the attached molecule, but it was tentatively predicted to be a methanethiol group based on its electron density, bond length, and temperature factors by X-ray diffraction studies. Thus, the modification of the second cysteine (Cys^{14}) observed in the [3Fe−4S] BtFd variant molecules is not unprecedented. More intriguingly, DgFd was purified from its native cell type in both [3Fe−4S] and [4Fe−4S] forms. In contrast, *in vitro* chemical reconstitution of the Fe−S cluster from apo-DgFd yields only the [4Fe−4S] type, whereas recombinant DgFd expressed in *E. coli* is purified predominantly as a [3Fe−4S] form (*18*, *41*). To date, modification of Cys^{11} in recombinant [3Fe−4S] DgFd has not been examined.

Physiological Considerations. Here, we have reported the purification and characterization of novel variant molecules of BtFd. Variants BtFd V-I and V-II were determined to be the BtFd−ACP complex and the BtFd−CoA complex,

respectively. BtFd V-III is most likely a dimer of BtFd connected by a disulfide bond. All of the variant molecules accommodate [3Fe−4S] clusters in place of the [4Fe−4S] cluster characteristic of the originally isolated BtFd. The crystal structure of the BtFd−CoA complex clearly demonstrates that this interaction involves a disulfide bond between the terminal thiol group of CoA and the Sγ of Cys^{14}, the residue which acts as the fourth ligand of [4Fe−4S] BtFd. Both ACP and CoA contain 4′-phosphopantetheine groups, which generally function as carriers of acyl groups (*44*). Because *E. coli* ACP lacks cysteine residues, the disulfide linkage in the BtFd−ACP complex should also involve the terminal sulfhydryl group of the prosthetic group. This brings up a question concerning the formation of these disulfide linkages *in vivo*: are these variant molecules indeed produced under the reducing conditions characteristic of the cytoplasm? When purified [4Fe−4S] BtFd was mixed with CoA (0.5 mM), neither deterioration of the [4Fe−4S] cluster, conversion to [3Fe−4S], nor formation of a disulfide bond was observed during a prolonged incubation of up to 1 month at 25 °C (data not shown). Therefore, the high degree of stability of [4Fe−4S] BtFd may suggest that the variant molecules are not simply artifacts produced during the purification steps. It is also noteworthy that the BtFd polypeptide has a high propensity for accommodating the [4Fe−4S] cluster, as evidenced by the fact that the [4Fe−4S] form was purified in much higher yield from the cells.

Two possibilities arise concerning how such variant molecules are formed in the cell. First, the variant molecules might be derived as a consequence of the high level of recombinant protein expression, where the situation that overwhelms the maturation system leads to exposed thiols that would not normally be present. Incidental modification of Cys^{14} may prevent the residue from serving as a ligand to the Fe−S cluster. During overproducing *Klebsiella pneumoniae* flavodoxin in *E. coli*, the occurrence of modified flavodoxin that is covalently bound to CoA through cysteine was reported (*45*). Second, the BtFd polypeptide may physically associate *in vivo* with CoA or ACP in a way that places the two reactive thiols in close proximity. Upon cell lysis, such an association would allow the formation of a disulfide linkage between the two molecules. In support of this view, a BtFd-glutathione adduct has not been detected in our preparations despite the fact that glutathione is the most abundant thiol in *E. coli* cells (*46*). In this context, it is noteworthy that previous studies have suggested that ACP, which normally functions in fatty acid biosynthesis (*44*), might play an active role in the formation of Fe−S clusters. An interaction between ACP and IscS, a cysteine desulfurase, has been demonstrated both by copurification of the native ACP−IscS complex from *E. coli* cells using several steps of conventional chromatography (*40*) and by rapid pull-down experiments using the recombinant proteins carrying affinity tags (*47*). The interaction involves a disulfide bond between the thiol groups of the 4′-phosphopantetheine of ACP and Cys^{328} of IscS, the essential residue for the activity (*22*, *48*). Furthermore, in fungi and animals, mitochondrial ACP is tightly associated with respiratory complex I (NADH: ubiquinone oxidoreductase), a membrane-bound multisubunit complex containing up to nine Fe−S clusters (*49*, *50*), and disruption of the gene for ACP in *Neurospora crassa* results in complex I deficiency, indicating that complex I cannot be assembled without ACP (*51*, *52*). Although the function of mitochondrial ACP is still elusive, the mutant phenotype may suggest that ACP is relevant to the Fe−S cluster biosynthesis. Regarding how the variant molecules of BtFd are derived, there is no convincing evidence at present that supports either one of the possibilities. The first one poses caution that overproducing Fe−S proteins may give side products, whereas the second one may provide a clue for the mechanism of the Fe−S protein maturation. Further studies are awaiting with much interest.

ACKNOWLEDGMENT

We thank Drs. Masahide Kawamoto and Hisanobu Sakai of JASRI for their aid with data collection using synchrotron radiation at SPring-8. The synchrotron-radiation experiments were performed at SPring-8 with the approval of the Japan Synchrotron Radiation Research Institute (JASRI; proposal number 2003B0488-NL1-np). We thank Dr. Shuji Tachibanaki (Graduate School of Frontier Biosciences, Osaka University) for amino-terminal sequencing of ACP and Dr. Tomoko Ohnishi (University of Pennsylvania) for an informative discussion.

REFERENCES

1. Matsubara, H., and Saeki, K. (1992) Structural and functional diversity of ferredoxins and related proteins, *Adv. Inorg. Chem. 38*, 223−280.
2. Sticht, H., and Rösch, P. (1998) The structure of iron−sulfur proteins, *Prog. Biophys. Mol. Biol. 70*, 95−136.
3. Grinberg, A. V., Hannemann, F., Schiffler, B., Müller, J., Heinemann, U., and Bernhardt, R. (2000) Adrenodoxin: Structure, stability, and electron-transfer properties, *Proteins 40*, 590−612.
4. Meyer, J. (2001) Ferredoxins of the third kind, *FEBS Lett. 509*, 1−5.
5. Fukuyama, K. (2004) Structure and function of plant-type ferredoxins, *Photosynth. Res. 81*, 289−301.
6. Fukuyama, K., Nagahara, Y., Tsukihara, T., Katsube, Y., Hase, T., and Matsubara, H. (1988) Tertiary structure of *Bacillus thermoproteolyticus* [4Fe−4S] ferredoxin: Evolutionary implications for bacterial ferredoxins, *J. Mol. Biol. 199*, 183−193.
7. Moulis, J.-M., Sieker, L. C., Wilson, K. S., and Dauter, Z. (1996) Crystal structure of the 2[4Fe−4S] ferredoxin from *Chromatium vinosum*: Evolutionary and mechanistic inferences for [3/4Fe−4S] ferredoxins, *Protein Sci. 5*, 1765−1775.
8. Fukuyama, K. (2001) in *Handbook of Metalloproteins* (Wieghardt, K., Ed.) pp 543−552.
9. Robbins, A. H., and Stout, C. D. (1989) Structure of activated aconitase: Formation of the [4Fe−4S] cluster in the crystal, *Proc. Natl. Acad. Sci. U.S.A. 86*, 3639−3643.
10. Beinert, H., Kennedy, M. C., and Stout, C. D. (1996) Aconitase as iron−sulfur protein, enzyme, and iron-regulatory protein, *Chem. Rev. 96* 2335−2373.
11. George, S. J., Armstrong, F. A., Hatchikian, E. C., and Thomson, A. J. (1989) Electrochemical and spectroscopic characterization of the conversion of the 7Fe into the 8Fe form of ferredoxin III from *Desulfovibrio africanus*: Identification of a [4Fe−4S] cluster with one non-cysteine ligand, *Biochem. J. 264*, 275−284.
12. Busch, J. L. H., Breton, J. L., Bartlett, B. M., Armstrong, F. A., James, R., and Thomson, A. J. (1997) [3Fe−4S] ↔ [4Fe−4S] cluster interconversion in *Desulfovibrio africanus* ferredoxin III: Properties of an Asp^{14} → Cys mutant, *Biochem. J. 323*, 95−102.
13. Conover, R. C., Kowal, A. T., Fu, W., Park, J.-B., Aono, S., Adams, M. W. W., and Johnson, M. K. (1990) Spectroscopic characterization of the novel iron−sulfur cluster in *Pyrococcus furiosus* ferredoxin, *J. Biol. Chem. 265*, 8533−8541.
14. Nielsen, M. S., Harris, P., Ooi, B. L., and Christensen, H. E. M. (2004) The 1.5 Å resolution crystal structure of [Fe_3S_4]-ferredoxin from the hyperthermophilic archaeon *Pyrococcus furiosus*, *Biochemistry 43*, 5188−5194.

15. Nagayama, K., Ozaki, Y., Kyogoku, Y., Hase, T., and Matsubara, H. (1983) Classification of iron−sulfur cores in ferredoxins by ^{1}H nuclear magnetic resonance spectroscopy, *J. Biochem. 94*, 893−902.
16. Morgan, T. V., Stephens, P. J., Devlin, F., Burgess, B. K., and Stout, C. D. (1985) Selective oxidative destruction of iron−sulfur clusters: Ferricyanide oxidation of *Azotobacter vinelandii* ferredoxin I, *FEBS Lett. 183*, 206−210.
17. Sridhar, V., Prasad, G. S., Burgess, B. K., and Stout, C. D. (1998) Crystal structures of ferricyanide-oxidized [Fe−S] clusters in *Azotobacter vinelandii* ferredoxin I, *J. Biol. Inorg. Chem. 3*, 140−149.
18. Moura, J. J. G., Moura, I., Kent, T. A., Lipscomb, J. D., Huynh, B. H., LeGall, J., Xavier, A. V., and Münck, E. (1982) Interconversions of [3Fe−3S] and [4Fe−4S] clusters: Mössbauer and electron paramagnetic resonance studies of *Desulfovibrio gigas* ferredoxin II, *J. Biol. Chem. 257*, 6259−6267.
19. Moura, J. J. G., LeGall, J., and Xavier, A. V. (1984) Interconversion from 3Fe into 4Fe clusters in the presence of *Desulfovibrio gigas* cell extracts, *Eur. J. Biochem. 141*, 319−322.
20. Kissinger, C. R., Sieker, L. C., Adman, E. T., and Jensen, L. H. (1991) Refined crystal structure of ferredoxin II from *Desulfovibrio gigas* at 1.7 Å, *J. Mol. Biol. 219*, 693−715.
21. Goodfellow, B. J., Macedo, A. L., Rodrigues, P., Moura, I., Wray, V., and Moura, J. J. G. (1999) The solution structure of a [3Fe−4S] ferredoxin: Oxidised ferredoxin II from *Desulfovibrio gigas*, *J. Biol. Inorg. Chem. 4*, 421−430.
22. Johnson, D., Dean, D. R., Smith, A. D., and Johnson, M. K. (2005) Structure, function, and formation of biological iron−sulfur clusters, *Annu. Rev. Biochem. 74*, 247−281.
23. Lill, R., and Mühlenhoff, U. (2005) Iron−sulfur-protein biogenesis in eukaryotes, *Trends Biochem. Sci. 30*, 133−141.
24. Mansy, S. S., and Cowan, J. A. (2004) Iron−sulfur cluster biosynthesis: Toward an understanding of cellular machinery and molecular mechanism, *Acc. Chem. Res. 37*, 719−725.
25. Takahashi, Y., and Tokumoto, U. (2002) A third bacterial system for the assembly of iron−sulfur clusters with homologs in archaea and plastids, *J. Biol. Chem. 277*, 28380−28383.
26. Ali, V., Shigeta, Y., Tokumoto, U., Takahashi, Y., and Nozaki, T. (2004) An intestinal parasitic protist, *Entamoeba histolytica*, possesses a non-redundant nitrogen fixation-like system for iron−sulfur cluster assembly under anaerobic conditions, *J. Biol. Chem. 279*, 16863−16874.
27. Tokumoto, U., Kitamura, S., Fukuyama, K., and Takahashi, Y. (2004) Interchangeability and distinct properties of bacterial Fe−S cluster assembly systems: Functional replacement of the *isc* and *suf* operons in *Escherichia coli* with the *nifSU*-like operon from *Helicobacter pylori*, *J. Biochem. 136*, 199−209.
28. Nakamura, M., Saeki, K., and Takahashi, Y. (1999) Hyperproduction of recombinant ferredoxins in *Escherichia coli* by coexpression of the ORF1-ORF2-*iscS*-*iscU*-*iscA*-*hscB*-*hscA*-*fdx*-ORF3 gene cluster, *J. Biochem. 126*, 10−18.
29. Takahashi, Y., and Nakamura, M. (1999) Functional assignment of the ORF2-*iscS*-*iscU*-*iscA*-*hscB*-*hscA*-*fdx*-ORF3 gene cluster involved in the assembly of Fe−S clusters in *Escherichia coli*, *J. Biochem. 126*, 917−926.
30. Fukuyama, K., Okada, T., Kakuta, Y., and Takahashi, Y. (2002) Atomic resolution structures of oxidized [4Fe−4S] ferredoxin from *Bacillus thermoproteolyticus* in two crystal forms: Systematic distortion of [4Fe−4S] cluster in the protein, *J. Mol. Biol. 315*, 1155−1166.
31. Bradford, M. M. (1976) A rapid and sensitive method for the quantitation of microgram quantities of protein utilizing the principle of protein-dye binding, *Anal. Biochem. 72*, 248−254.
32. Laemmli, U. K. (1970) Cleavage of structural proteins during the assembly of the head of bacteriophage T4, *Nature 227*, 680−685.
33. Davis, B. J. (1964) Disc electrophoresis. II. Method and application to human serum proteins, *Ann. N.Y. Acad. Sci. 121*, 404−427.
34. Otwinowsky, Z., and Minor, W. (1997) Processing of X-ray diffraction data collected in oscillation mode, *Methods Enzymol. 276*, 307−326.
35. Vagin, A., and Teplyakov, A. (2000) An approach to multi-copy search in molecular replacement, *Acta Crystallogr., Sect. D: Biol. Crystallogr. 56*, 1622−1624.
36. Brünger, A. T., Adams, P. D., Clore, G. M., DeLano, W. L., Gros, P., Grosse-Kunstleve, R. W., Jiang, J.-S., Kuszewski, J., Nilges, M., Pannu, N. S., Read, R. J., Rice, L. M., Simonson, T., and Warren, G. L. (1998) Crystallography and NMR system: A new software suite for macromolecular structure determination, *Acta Crystallogr., Sect. D: Biol. Crystallogr. 54*, 905−921.
37. Jones, T. A., Zou, J.-Y., Cowan, S. W., and Kjeldgaard, M. (1991) Improved methods for building protein models in electron density maps and the location of errors in these models, *Acta Crystallogr., Sect. A: Found. Crystallogr. 47*, 110−119.
38. Laskowski, R. A., MacArthur, M. W., Moss, D. S., and Thornton, J. M. (1993) PROCHECK: A program to check the stereochemical quality of protein structures, *J. Appl. Crystallogr. 26*, 283−291.
39. Hill, R. B., MacKenzie, K. R., Flanagan, J. M., Cronan, J. E., Jr., and Prestegard, J. H. (1995) Overexpression, purification, and characterization of *Escherichia coli* acyl carrier protein and two mutant proteins, *Protein Expression Purif. 6*, 394−400.
40. Flint, D. H. (1996) *Escherichia coli* contains a protein that is homologous in function and N-terminal sequence to the protein encoded by the *nifS* gene of *Azotobacter vinelandii* and that can participate in the synthesis of the Fe−S cluster of dihydroxy-acid dehydratase, *J. Biol. Chem. 271*, 16068−16074.
41. Rodrigues, P., Graça, F., Macedo, A. L., Moura, I., and Moura, J. J. G. (2001) Characterization of recombinant *Desulfovibrio gigas* ferredoxin, *Biochem. Biophys. Res. Commun. 289*, 630−633.
42. Mullinger, R. N., Cammack, R., Rao, K. K., Hall, D. O., Dickson, D. P. E., Johnson, C. E., Rush, J. D., and Simopoulos, A. (1975) Physicochemical characterization of the four-iron-four-sulphide ferredoxin from *Bacillus stearothermophilus*, *Biochem. J. 151*, 75−83.
43. Beinert, H., and Thomson, A. J. (1983) Three-iron clusters in iron−sulfur proteins, *Arch. Biochem. Biophys. 222*, 333−361.
44. White, S. W., Zheng, J., Zhang, Y.-M., and Rock, C. O. (2005) The structural biology of type II fatty acid biosynthesis, *Annu. Rev. Biochem. 74*, 791−831.
45. Thorneley, R. N., Abell, C., Ashby, G. A., Drummond, M. H., Eady, R. R., Huff, S., Macdonald, C. J., and Shneier, A. (1992) Posttranslational modification of *Klebsiella pneumoniae* flavodoxin by covalent attachment of coenzyme A, shown by ^{31}P NMR and electrospray mass spectrometry, prevents electron transfer from the *nifJ* protein to nitrogenase. A possible new regulatory mechanism for biological nitrogen fixation, *Biochemistry 31*, 1216−1224.
46. Li, Y., Wei, G., and Chen, J. (2004) Glutathione: A review on biotechnological production, *Appl. Microbiol. Biotechnol. 66*, 233−242.
47. Gully, D., Moinier, D., Loiseau, L., and Bouveret, E. (2003) New partners of acyl carrier protein detected in *Escherichia coli* by tandem affinity purification, *FEBS Lett. 548*, 90−96.
48. Mihara, H., and Esaki, N. (2002) Bacterial cysteine desulfurases: Their function and mechanisms, *Appl. Microbiol. Biotechnol. 60*, 12−23.
49. Runswick, M. J., Fearnley, I. M., Skehel, J. M., and Walker, J. E. (1991) Presence of an acyl carrier protein in NADH:ubiquinone oxidoreductase from bovine heart mitochondria, *FEBS Lett. 286*, 121−124.
50. Sackmann, U., Zensen, R., Röhlen, D., Jahnke, U., and Weiss, H. (1991) The acyl-carrier protein in *Neurospora crassa* mitochondria is a subunit of NADH:ubiquinone reductase (complex I), *Eur. J. Biochem. 200*, 463−469.
51. Schneider, R., Massow, M., Lisowsky, T., and Weiss, H. (1995) Different respiratory-defective phenotypes of *Neurospora crassa* and *Saccharomyces cerevisiae* after inactivation of the gene encoding the mitochondrial acyl carrier protein, *Curr. Genet. 29*, 10−17.
52. Schulte, U. (2001) Biogenesis of respiratory complex I, *J. Bioenerg. Biomembr. 33*, 205−212.
53. Collaborative Computational Project, N. (1994) The CCP4 suite: Programs for protein crystallography, *Acta Crystallogr., Sect. D: Biol. Crystallogr. 50*, 760−763.

BI0508441